Ionics (2015) 21:3209–3215
DOI 10.1007/s11581-015-1493-0

ORIGINAL PAPER

Electrochemical kinetic properties of AB_5-type hydrogen storage alloys with chemically deposited polypyrrole

Lin Hu[1] · **Jianping Li**[1] · **Wei Yang**[1]

Received: 19 March 2015 / Revised: 25 May 2015 / Accepted: 21 June 2015 / Published online: 4 July 2015

Abstract $La_{0.65}Ce_{0.25}Pr_{0.02}Nd_{0.08}Ni_{3.85}Mn_{0.39}Co_{0.73}Al_{0.31}$ AB_5-type alloy was modified via the method of a simple chemical oxidative polymerization of pyrrole (Py) directly occurring on the surface of alloy particles. Field emission scanning electron microscopy and Fourier transform infrared spectroscopy revealed spongy polypyrrole (PPy) films uniformly and continuously deposited on the surface of the alloy particles. The PPy films possessed superior electrochemical redox reversibility, thus facilitating hydrogen protons transferring from electrolyte to electrode interface. Moreover, the PPy films exhibited prominent anti-corrosion properties and reduced the pulverization of the alloy particles. The PPy-coated alloy received remarkable enhancement in rate capability and cyclability compared to those of the bare alloy. Due to the PPy films, the high-rate dischargeability at a discharge current density of 1500 mA g^{-1} (HRD_{1500}) significantly increased from 18 to 31.6 %, and the capacity retention rate after 200 cycles (S_{200}) increased from 84.2 to 89.8 %. Meanwhile, the PPy coatings decreased the charge transfer resistance and increased the hydrogen diffusion rate of the alloys, which well conformed with the HRD results.

Keywords Hydrogen storage alloy · Polypyrrole · Surface treatment · Electrochemical characteristics

✉ Lin Hu
hulin912@sina.com

[1] School of Materials and Chemical Engineering, Xi'an Technological University, Xi'an 710021, China

Introduction

In recent years, the rapid development of electric vehicles (EV) and hybrid electric vehicle (HEV) has drawn much attention to improve existing metal hydride/nickel (MH-Ni) secondary batteries to achieve the demands that are high power, excellent cycle stability, and low cost [1, 2]. Rare earth-based AB_5-type alloys, the most commercial negative materials, have been extensively investigated; however, the main drawback of the AB_5-type alloys is the poor performance of significant deterioration in practical applications [3]. Many efforts, such as optimization of the alloy compositions, acid treatment, alkali treatment, and microencapsulation with Ni, Cu, Pd, etc. [4–8], have been made to overcome the above shortcomings and hence to improve the comprehensive electrochemical performance. Surface modification by encapsulation with conducting polymer overlayer is one of the most efficient solutions, which can catalyze the dissociative chemisorption and associative desorption of H and improves the catalytic activity of the surface [9].

Conducting polymer contains polyaniline (PANI), polypyrrole (PPy), and so on. Up to now, PANI has been widely investigated for their resistance to corrosion and good stability to enhance the electrochemical performance of hydrogen alloys. For instance, Shen et al. applied PANI-coated technique for hydrogen storage alloys by electrodeposition and chemical deposition [10]. In such cases, the electrochemical kinetics of surface-modified hydrogen storage alloys is dramatically ameliorated. However, aniline monomers are somewhat environmentally and healthily hazardous.

Polypyrrole (PPy), another normal polymer, is a suitable alternative for the capacitor [11], chemical pickup [12], bioelectrode [13], and conductive and anti-corrosion materials [14, 15] in conducting polymers. It is attractive due to the simplicity of its synthesis, non-toxicity, high stability,

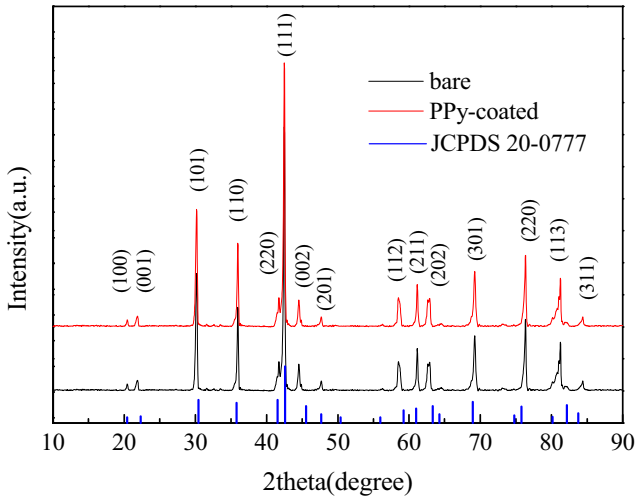

Fig. 1 XRD of bare alloy and PPy-coated alloy

environmental friendliness, and ability to be scaled up to industrial production with relative ease. Ma et al. [16] designed a sulfur cathode with polypyrrole warped mesoporous carbon/sulfur composite. The PPy coatings are beneficial for the enhanced conductivity of cathode and the suppression of active materials from dissolution. Considering that PPy films can be grown easily on different substrates using chemical methods, in this work, we modified the surface of a rare earth-based AB_5-type alloy using chemical modification, aiming to improve the catalytic activity and anti-corrosion properties of the hydrogen storage alloy. This study presents our preliminary results on the surface modification of the rare earth-based AB_5-type alloy with PPy by chemical deposition. The morphology, electrochemical properties, and kinetics of the alloy were systematically investigated, and remarkable enhancement was obtained.

Experimental

The rare earth-based AB_5-type alloy $La_{0.65}Ce_{0.25}Pr_{0.02}Nd_{0.08}Ni_{3.85}Mn_{0.39}Co_{0.73}Al_{0.31}$ was prepared using induction melting for constituent metals (purity, ≥99.5 %) in an argon atmosphere. The as-cast ingot was subsequently annealed at 1173 K for 8 h. And then, the annealed ingots were mechanically crushed and ground to particles of 200–400 mesh size for further treatment. The alloy powders in mass of 2 g were immersed into a mixed aqueous solution of 50 mL of pyrrole (c=0.3 mol L^{-1}) and 30 % H_2O_2 (c=0.2 mol L^{-1}), which was constantly stirred in the air for various times (t=0, 5, 8, and 10 min). Subsequently, the treated alloy powders were washed, filtered, and dried in vacuum at 60 °C for 4 h.

The structural characterization was performed by X-ray powder diffraction (XRD) with a Rigaku D/Max 2500PC X-ray diffractometer (Cu Ka radiation), ranging from 10 to 90°. The surface morphology of alloy particles was observed by field emission scanning electron microscopy (FE-SEM) on a HITACHI S-4800 microscope. Infrared spectroscopy measurements were performed using an E55 + FRA106 Fourier transform infrared (FT-IR) spectrometer. Thermogravimetric (TG) curves were obtained from 25 to 700 °C, at 10 °C min^{-1}, under a purified argon atmosphere using a Shimadzu DTG-60A system.

The testing electrodes were prepared by mixing the carbonyl nickel powders (0.75 g) and alloy powders (0.15 g). The mixed powders were cold pressed into a tablet with 10 mm in diameter under a pressure of 15 MPa. Test cells were assembled using the prepared electrode as working electrode, $Ni(OH)_2$/NiOOH electrode as counter electrode, Hg/HgO electrode as reference electrode, and 6 mol L^{-1} KOH solution as electrolyte. All the electrochemical and kinetic measurements were performed by a DC-5 battery test instrument at ambient temperature (298 K). During the charge/discharge processes, the electrodes were fully charged for 8 h at a current density of 60 mA g^{-1} and then discharged at the same current to the cutoff potential of −0.6 V (versus Hg/HgO reference electrode). After the electrodes reached the maximum capacity, they were charged and discharged with a current density of 300 mA g^{-1} to evaluate the electrochemical cycling stability. For the charge retention (CR) test, the testing electrodes were fully charged and then lay aside for 24 h at 298 K. The

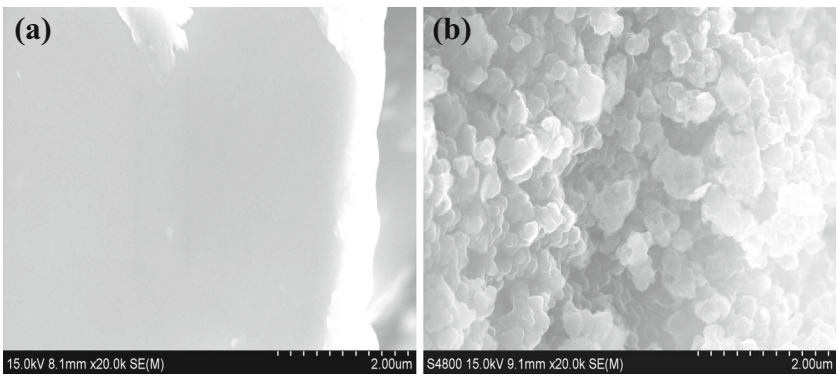

Fig. 2 FE-SEM photographs of **a** bare alloy and **b** PPy-coated alloy particle surface

discharge capacity was measured after the standing. For the high-rate dischargeability (HRD) measurements, the discharge capacities were performed at various discharge current densities (I_d).

The kinetic measurements were performed based on the followed parameters, and the electrodes were fully activated before these measurements. At 50 % depth of discharge (DOD), the linear polarization and the anode polarization curves were measured on ZF-9 potentiostat by scanning electrode potential at a rate of 5 mV min^{-1} and 5 mV s^{-1} from −5 to 5 mV and from 0 to 1500 mV (versus open circuit potential). Electrochemical impendence spectroscopy (EIS) studies were conducted using a CHI660C electrochemical analyzer/working platform. The EIS spectra of the electrodes were obtained in the frequency range from 10 kHz to 5 mHz with an ac amplitude of 5 mV under the open circuit condition. In the potential static step discharge, the electrodes were in fully charged state with +500 mV potential steps for 3600 s.

Results and discussion

Material characterization

Figure 1 shows the XRD patterns of bare and PPy-coated alloy particles. The AB_5-type alloy contains the single $LaNi_5$ phase. PPy structure is not observed due to its low content. No extra peaks were detected, indicating that no changes in the structure of the AB_5-type alloy occurred after being coated with PPy. Figure 2 shows FE-SEM images of bare and PPy-coated alloy particles. The bare alloy particles have smooth surfaces and sharp edges. For the PPy-coated alloys, the spongy-shaped PPy films deposit on the surface of alloy particles, which distribute continuously and evenly. The FT-IR spectra of the bare and PPy-coated alloy particles are shown in Fig. 3. The characteristic peaks appeared at 1537 and 1450 cm^{-1} (fundamental vibrations of the pyrrole rings) and at 906 cm^{-1} (C–C out-of-plane ring deformation vibration). Combined with SEM results, it can be inferred that PPy coatings are deposited on the alloy surface by chemical deposition. The procedure followed for coating the alloy particles with PPy is similar to the ion-pairing mechanism proposed by Zotti et al. [17]; each pyrrole monomer first loses an electron and turns into a cationic radical due to oxidation, and then, the ion pair complex reduces the electrostatic repulsion between two cation radicals, which benefits the coupling of the two cation radicals for polymerization. Figure 4 shows the TG curve for PPy-coated alloys. The curve depicts mass losses in two consecutive steps between 25 and 700 °C. The first mass loss from 25 to 130 °C occurred very rapidly and can be attributed to the loss of bulk water in the alloy, whereas the second mass loss from 130 to 500 °C can be attributed to the loss of PPy. The quantity of PPy lost in this step corresponds to 2.51 wt% of the PPy-coated alloy.

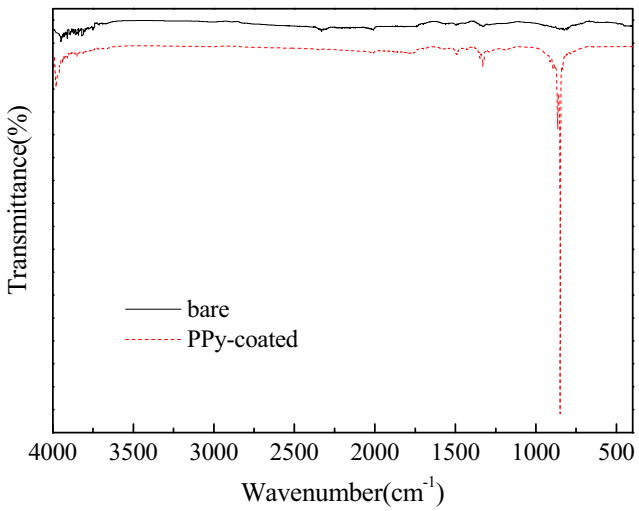

Fig. 3 FT-IR spectra of the bare and PPy-coated AB_5-type alloys

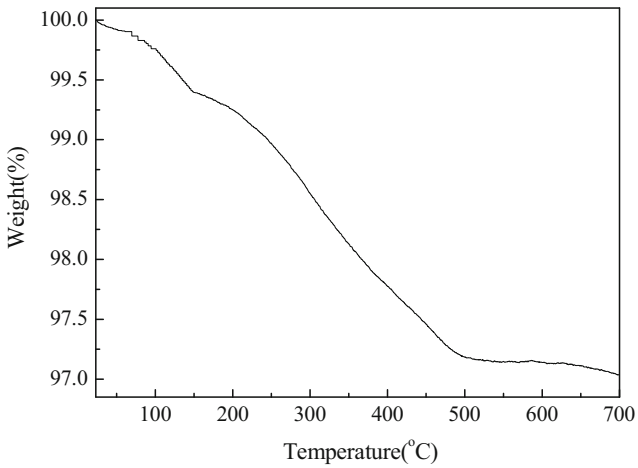

Fig. 4 TG of the electroless deposited PPy-coated alloy

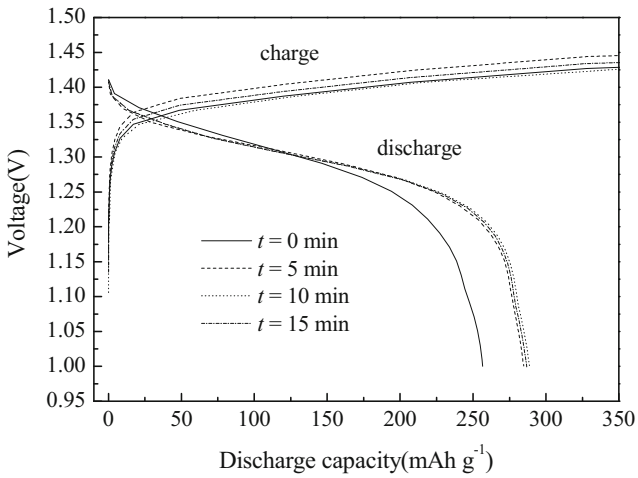

Fig. 5 Charge–discharge curves of the bare and PPy-coated AB_5-type alloys

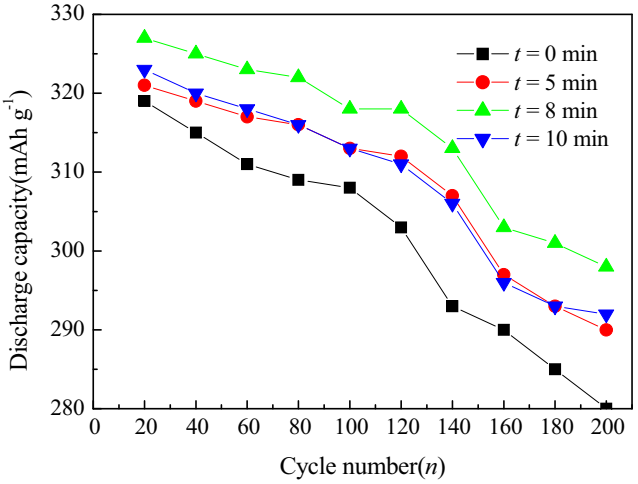

Fig. 6 Discharge capacity of PPy-coated AB_5-type alloy vs. cycle number in various times

Electrochemical and kinetic characteristics

Initial charge and discharge curves of the bare and PPy-coated alloy electrodes are presented in Fig. 5. It can be seen that the electrodes show a long and flat discharge voltage plateau, and the plateau becomes longer and higher after coated with PPy. The initial discharge capacities of the electrodes are 257 mAh g^{-1} (bare), 285 mAh g^{-1} (t=5 min), 289 mAh g^{-1} (t=8 min), and 287 mAh g^{-1} (t=10 min), respectively. We also carried out the charge/discharge measurements for PPy particles, carbonyl nickel, and PPy + carbonyl nickel. Results showed that the discharge capacity of these electrodes is approximately zero. Compared to that of alloy electrodes, it is small enough to be ignored. Figure 6 shows the cyclic stability of the bare and PPy-coated alloys. The rate capacity retention at the 200th charge/discharge cycle was calculated as follows:

$$S_{200}(\%) = C_{200}/C_{\max} \times 100\% \quad (1)$$

Herein, C_{200} is the discharge capacity at the 200th cycle; $C_{\max}$ is the maximum discharge capacity, and S_{200} is the capacity retention rate. As shown in Fig. 6, C_{200} increased from 280 mAh g^{-1} (0 min) to 298 mAh g^{-1} (8 min) but decreased to 292 mAh g^{-1} (10 min) in the alloy electrodes; moreover, S_{200} for the PPy-coated alloy increased slightly to 89.8 % (8 min) compared to 84.2 % for the bare alloy. It is well known that dissolution loss of active materials can cause the decay of the discharge capacity. The PPy films on the alloy surface, born with good anti-corrosion properties, can hinder the alloy particles directly exposed to alkaline electrolyte and mitigate corrosion of active materials to some extent. It can be deduced that the PPy films can enhance the cyclic stability of alloy electrodes.

To further investigate the effect of the PPy coatings formed on the alloy surface, a surface morphology of the bare and PPy-coated alloy after 200 cycles was performed by FE-SEM. Figure 7 shows FE-SEM images of the bare and PPy-coated alloy electrodes after 200 cycles, clearly reflecting the effects of treatment. The bare alloy particles were pulverized severely, whereas the surfaces of the PPy-coated alloys were uniformly covered by the spongy films to maintain particle integration, as shown in Fig. 7b. Microencapsulation by PPy provides coverage on the alloy particle surface, which helps prevent corrosion and oxidation of the hydrogen storage alloy. Furthermore, the spongy PPy films on alloy surfaces lead to a decrease in contact resistance, which is beneficial for the interfacial electrochemical reactions of alloy electrodes [18]. These results suggest that improvements in cycling stability can be attributed to the PPy films deposited on the hydrogen storage alloy particles.

To prove the anti-corrosion properties, the study of the corrosion behaviors of the bare and PPy-coated alloy electrodes was performed by the technique of potentiodynamic polarization. The obtained data were plotted, the Tafel curves shown in Fig. 8. It can be found that the corrosion current density decreased from 31.8 to 24.5 mA cm^{-2}, which demonstrates that the PPy-coated alloy electrode has a better anti-corrosion ability. It demonstrates that the PPy coating possesses a good anti-corrosion property.

Figure 9 shows the charge retention (CR) of PPy-coated alloy electrodes at various treatment times. CR can be calculated as follows:

$$CR(\%) = 2C_b/(C_a + C_c) \times 100\% \quad (2)$$

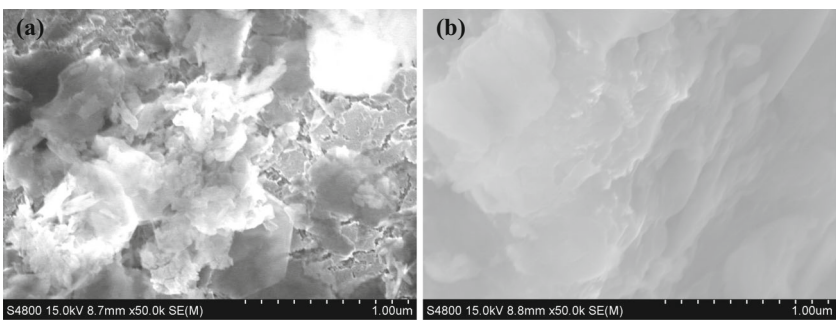

Fig. 7 FE-SEM photographs of **a** bare alloy and **b** PPy-coated alloy particle surface after 200 cycles

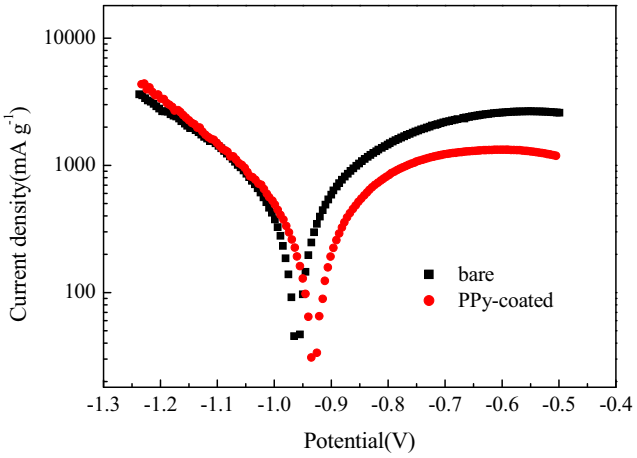

Fig. 8 Tafel curves of the bare and PPy-coated AB_5-type alloys

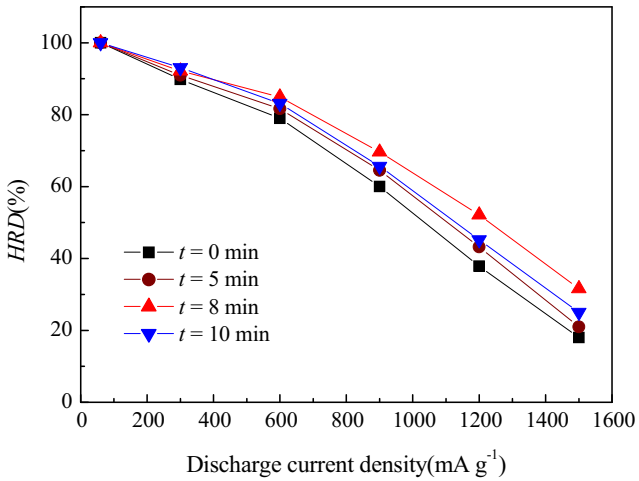

Fig. 10 HRD of the bare and PPy-coated alloys in various times

where C_b is the discharge capacity after laying out open circuits for 24 h at 298 K, and C_a and C_c are the discharge capacities before and after C_b is tested, respectively. As shown in Fig. 9, the CR of PPy-coated alloy electrodes increased from 87.4 to 93.8 %. CR is an important property for the unloaded condition of batteries, and it must be as high as possible for practical applications. During electroless deposition, the spongy PPy film formed on the surface of alloy particles can effectively inhibit H from spilling over from the surface, thereby reducing the reversibility of capacity loss.

Figure 10 shows the HRD of PPy-coated alloy electrodes. HRD is expressed as follows:

$$\mathrm{HRD}(\%) = C_d/C_{60} \times 100\% \quad (3)$$

where C_d is the discharge capacity at discharge current density I_d, and C_{60} is the discharge capacity at 60 mA g^{-1}. The HRD at 1500 mA g^{-1} increases distinctly from 18.0 to 31.6 % with t ranging from 0 to 8 min, almost 14.0 % higher than the bare alloy. But when t increases to 10 min, the HRD is enhanced as well, though it slightly decreases to 25.0 %. It is influenced by the diffusion rate of H in the bulk and the charge transfer rate on the alloy surface. According to the electrochemical redox reversibility characteristic of PPy, a mass of H between PPy and the alloy surface exists in the oxidation–reduction process, which speeds up charge transference on the electrode–electrolyte interface and the hydrogen diffusion of the network structure of polymer films [19]. Herein, we carried out a series of kinetic experiments with bare and PPy-coated alloy electrodes at t=8 min.

Figure 11 shows the linear polarization curves of the bare and PPy-coated alloy electrodes at 50 % DOD. The exchange current density (I_0), which characterizes the charge transfer rate on the surface of the electrodes, is calculated as follows [20]:

$$I_0 = RTI/F\eta \quad (4)$$

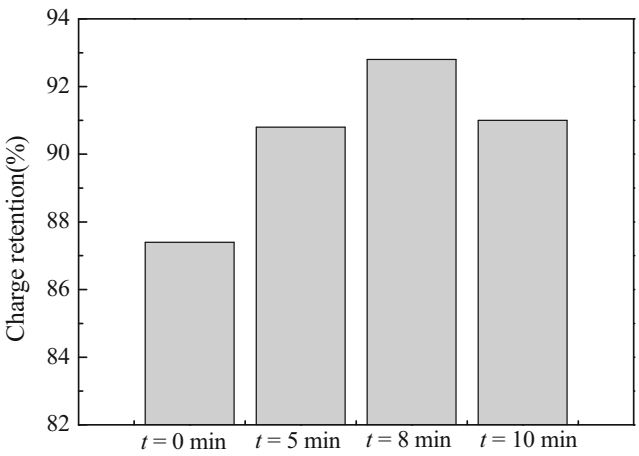

Fig. 9 Charge retention of the bare and PPy-coated AB_5-type alloys in various times

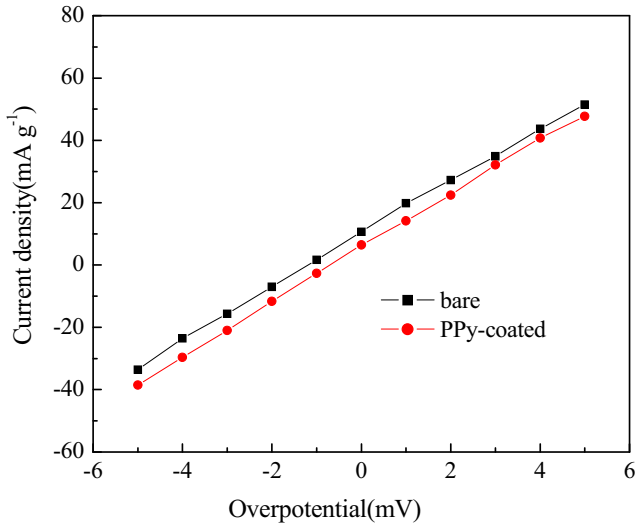

Fig. 11 Linear polarization curves of the bare and PPy-coated alloy electrodes

Table 1 Kinetic properties of the bare and PPy-coated AB_5-type alloy electrodes

Samples	I_0 (mA g^{-1})	I_L (mA g^{-1})	R_{ct} (mΩ)	D ($\times 10^{-13}$ cm^2 s^{-1})
Bare	217.8	2230	718	9.89
PPy coating	223.5	2308	690	11.80

where I, T, R, F, and η are the applied current density (A), the absolute temperature (K), the gas constant (J mol^{-1} K^{-1}), the Faraday constant (C mol^{-1}), and the total overpotential (V), respectively. The high value of I_0 is supported by good kinetics for hydriding/dehydriding. The exchange current density has been found to increase owing to the electroless deposition of macromolecule polymer on the surface of alloy particles. The calculated results are listed in Table 1.

The HRD of the alloy was dominated by the electrochemical kinetics of the charge transfer reaction at the electrode–electrolyte interface and the hydrogen diffusion at the bulk electrode, which can be expressed as limiting current density I_L [21]. Figure 12 shows the anode polarization curves of the bare and PPy-coated alloy electrodes at 50 % DOD and 298 K. During the anodic polarization process, the anodic current increased by degrees and reached a maximum with overpotential increase. Figure 12 also shows the I_L values of the alloy electrodes listed in Table 1.

Electrochemical impedance was measured at 50 % DOD and 298 K, and the Nyquist plots of the bare and PPy-coated alloy electrodes are shown in Fig. 13. Each spectrum is composed of two semicircles followed by a straight line at the low-frequency range. Kuriyama et al. [22] reported that the radius of the smaller semicircle is almost unchanged and that the radius of the larger semicircle decreases after PPy coating, indicating that charge transfer resistance (R_{ct}) decreases.

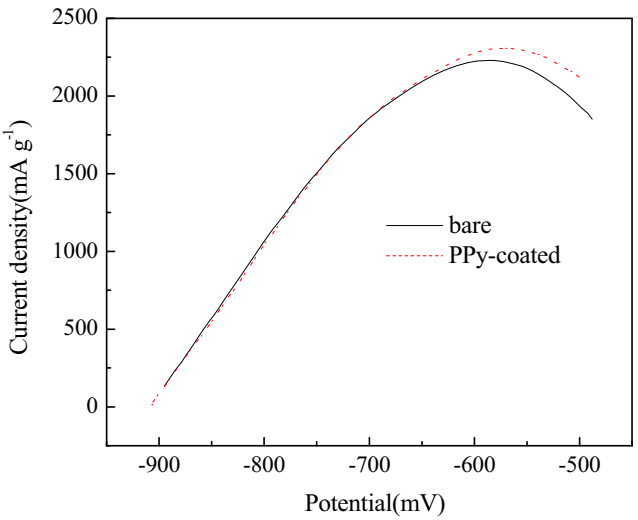

Fig. 12 Anodic polarization curves of the bare and PPy-coated alloy electrodes at 50 % DOD

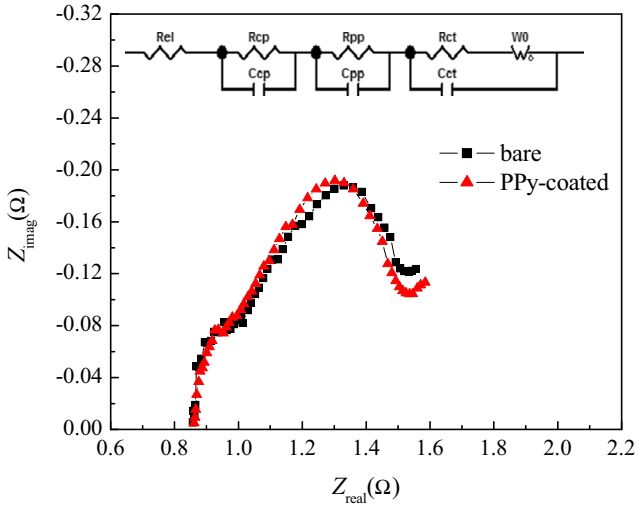

Fig. 13 Nyquist plots of the bare and PPy-coated alloy electrodes at 50 % DOD

These findings are consistent with the results we obtained using Z-View (Table 1). After PPy coating, R_{ct} became smaller than the bare alloy, thus giving the PPy-coated alloy a smaller charge transfer resistance at the surface of the electrode.

Furthermore, the hydrogen diffusion coefficient can be calculated from the potential step method. Figure 14 shows the correspondence of anodic current density to discharge time of the bare and PPy-coated alloy electrodes. The semilogarithmic value of the anodic current (log i) revealed an approximately linear dependence on time (t). The surface concentration of hydrogen is approximately zero under these circumstances; thus, the electrode reaction will be dominated by hydrogen diffusion in the alloy bulk. The hydrogen diffusion coefficient D in the bulk of the alloy can be calculated as follows [21]:

$$\log i = \log\left(6FD(C_0 - C_s)/da^2\right) - \pi^2 Dt/2.303a^2 \quad (5)$$

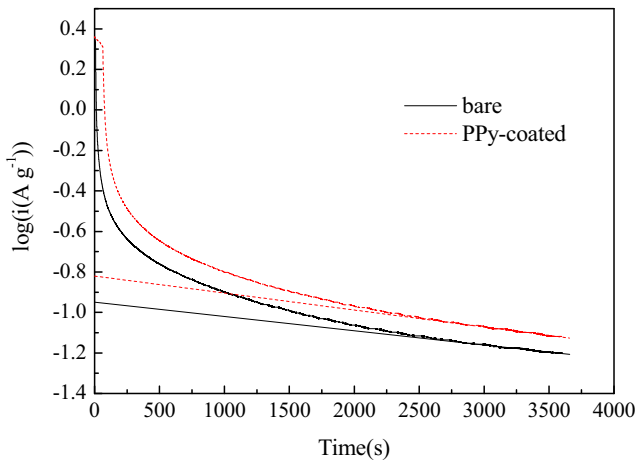

Fig. 14 Correspondence of anodic current density vs. discharge time of the bare and PPy-coated alloy electrodes

where i is the anodic current density (mA g^{-1}), D is the hydrogen diffusion coefficient (cm^2 s^{-1}), d is the density of the alloy (g cm^{-3}), C_0 is the initial hydrogen concentration in the bulk of the alloy (mol cm^{-3}), C_s is the surface hydrogen concentration of the alloy (mol cm^{-3}), t is the discharge time (s), and a is the radius of the alloy particles (13 μm in this case). D can be calculated using Eq. (5), and its values are summarized in Table 1. These results clearly indicate that D increases, which shows that the hydrogen diffusion rate in the alloy bulk increases with PPy coating, and are supported by the results of the HRD measurements.

Conclusions

With a simple and efficient way, the PPy-coated alloys were successfully obtained by the method of chemical oxidative polymerization of pyrrole (Py) on the alloy surface. The unique spongy-shaped PPy films were continuously formed on the alloy surface, which remarkably improve the electrochemical performance of AB_5-type alloys. The high-rate dischargeability (HRD_{1500}) significantly increased from 18 to 31.6 %, and the capacity retention rate after 200 cycles (S_{200}) increased from 84.2 to 89.8 %. The enhanced performance is attributed to the synergistic effect of the two reasons as follows. Firstly, the PPy films with superior electrochemical redox reversibility provide a fast electron transfer path, thus facilitating hydrogen protons diffusion. Secondly, the PPy films inhibit the alloy particles from oxidation and pulverization in the electrolyte.

Acknowledgments This project was financially supported by the Fundamental Research Funds for the Natural Science Foundation of China (No. 51201176).

References

1. Liu YF, Cao YH, Huang L, Gao MX, Pan HG (2011) J Alloys Compd 509:675
2. Pan CC, Yang SL, Yu RH, Shi J, Nakamura Y (2010) J Rare Earth 28:286
3. Lee HJ, Yang DC, Park CJ, Park CN, Jang HJ (2009) Int J Hydrog Energy 34:481
4. Zhang JL, Han SM, Li Y, Liu JJ, Yang SQ, Zhang L, Wang JD (2013) J Alloys Compd 581:693
5. Raju M, Ananth MV, Vijayaraghavan L (2009) J Alloys Compd 475:664
6. Bai TY, Han SM, Lin ZX, Zhang Y, Li Y, Zhang WC (2009) Mater Chem Phys 117:173
7. Li Y, Han SM, Liu ZP (2010) Int J Hydrog Energy 35:12858
8. Yang SQ, Liu HP, Han SM, Li Y, Shen WZ (2013) Appl Surf Sci 271:210
9. Wang BP, Zhao LM, Cai CS, Wang SX (2014) Int J Hydrog Energy 39:10374
10. Shen WZ, Han SM, Li Y, Yang SQ, Miao Q (2012) Appl Surf Sci 258:6316
11. Muthulakshmi B, Kalpana D, Pitehumani S (2006) J Power Sources 158:1533
12. Fang Y, Ngin TS, Hailin G (1996) Sens Actuators B Chem 32:33
13. Konga Y, Wang CY, Yang Y, Too CO, Wallace GG (2012) Synth Met 162:584
14. Herrasti P, Rio AI, Recio J (2007) Electrochim Acta 52:6496
15. Qi XN, Vetter C, Harper AC, Gelling VJ (2008) Prog Org Coat 63: 345
16. Ma GQ, Wen ZY, Jin J, Lu Y, Rui K, Wu XW, Wu MF, Zhang JC (2014) J Power Sources 254:353
17. Zotti G, Schiavon G, Zecchin S, Sannicolo' F, Brenna E (1995) Chem Mater 7:1464
18. Sun A, Li Z, Wei T (2009) Sens Actuators B Chem 142:197
19. Notten PHL, Hokkeling P (1991) J Electrochem Soc 138:1877
20. Ratnakumar BV, Witham C, Bowman RCJ (1996) J Electrochem Soc 143:2578
21. Kuriyama N, Sakai T, Miyamura H, Uehara I, Ishikawa H, Iwasaki T (1993) J Alloy Compd 202:183
22. Zheng G, Popov BN, White RE (1995) J Electrochem Soc 142: 2695